Global uncertainty and sensitivity analysis of a reduced chemical kinetic mechanism of a gasoline, n-butanol blend in a high pressure rapid compression machine.

AGBRO, Edirin

GLOBAL UNCERTAINTY AND SENSITIVITY ANALYSIS OF A REDUCED CHEMICAL KINETIC MECHANISM OF A GASOLINE, *N*-BUTANOL BLEND IN A HIGH PRESSURE RAPID COMPRESSION MACHINE

Edirin Agbro*
School of Chemical and Process Engineering, University of Leeds, Leeds, LS2 9JT, United Kingdom

ABSTRACT

A detailed evaluation of a recently developed combined n-butanol/toluene reference fuel (TRF) reduced chemical kinetic mechanism describing the low temperature oxidation of n-butanol, gasoline and a gasoline/n-butanol blend was performed using both global uncertainty and sensitivity methods with ignition delays as the predicted output for the temperature range 678 - 858 K, and an equivalence ratio of 1 at 20 bar. The results obtained when incorporating the effects of uncertainties in forward rate constants in the simulations, showed that uncertainties in predicting key target quantities for the various fuels studied are currently large but driven by few reactions. Global sensitivity analysis of the mechanism based on predicted ignition delays of stoichiometric TRF mixtures, showed the toluene + OH route = phenol + CH_3 to be among the most dominant pathways in terms of the predicted output uncertainties but an update on the mechanism based on data from a recent study led to the toluene + OH hydrogen abstraction reaction becoming the most dominant reaction as expected. For the TRF/n-butanol blend, hydrogen abstraction reactions by OH from n-butanol appear to be key in predicting the effect of blending. Uncertainties in the temperature dependence of relative abstraction rates from the α and γ sites may still be present within current mechanisms, and in particular may affect the ability of the mechanisms to capture the low temperature delay times for n-butanol. Further studies of the product channels for n-butanol + OH for temperatures of relevance to combustion applications could help to improve current mechanisms. At higher temperatures, the reactions of HO_2 and that of formaldehyde with OH also became critical and attempts to reduce uncertainties in the temperature dependent rates of these reactions would be useful.

KEYWORDS: *n-butanol, ignition delay, blending, global sensitivity, uncertainty quantification*

1.0 INTRODUCTION

In order to continue to use liquid fuels at lower emission levels, modern combustion devices need to become significantly more efficient. Bio-derived alcohols such as methanol, ethanol and butanol are currently being projected as suitable blends for fossil-

* Corresponding author e-mail: edirigbo@yahoo.com

derived fuels in order to reduce their overall carbon footprint (Agarwal, 2007). The similarity of their physical and chemical properties to those of fossil-derived fuels make them compatible with modern engines, particularly when used as blends (Sarathy et al., 2014, Szwaja and Naber, 2010). Ethanol has been used extensively and can be used at low blending ratios with gasoline without requiring engine modifications. However, there is presently some support for biobutanol (*n*-butanol or 1-butanol) as a potential replacement for ethanol in spark ignition (SI) and compression ignition (CI) engines due to its numerous similarities with gasoline (Table 1) and advantages over ethanol. Due to its higher energy density, butanol offers better fuel economy when blended with gasoline compared to ethanol. With many properties (i.e. lower heating value and stoichiometric air-fuel ratio) that are more similar to gasoline than ethanol, butanol can be blended with gasoline at higher concentrations without the need for engine retrofitting or modification (Wigg, 2011). In one of the studies reported in the literature (Dernotte et al., 2009) up to 80 % of butanol by volume was blended with gasoline. Other advantages of butanol over ethanol include its tolerance for water contamination in gasoline and less tendency to corrosion allowing it to be transported with existing distribution fuel pipelines.

While renewable bio-derived liquid fuels and their blends with conventional fuels (i.e. *n*-butanol blended with gasoline) are a promising option for achieving a lower carbon footprint, a wider penetration and sensible use of these fuels in internal combustion engines requires first and foremost, an in-depth understanding of the performance of the fuel blends under a wide range of operating conditions. Achieving this using an experimental approach for a range of fuel blends is currently quite challenging due to the cost involved, hence the need for a computer approach. Computer simulation and analysis provides the ability to relatively solve the complex problems related to these new and completely different fuels cheaply and quickly without having to go into the rigors of very expensive and time consuming experimental testing (Baulch, 1997). Where experimental measurements are difficult or impossible, the wide range of data provided through computer modelling can also be effectively utilised for the design, testing and control of new and conventional combustion technologies required to use alternative fuels optimally. However, a successful application of computational strategies depends on the availability of reliable and detailed well validated chemical kinetic mechanisms of the various fuels/fuel blends as input in computer simulations for characterization of the engine combustion processes.

Gasoline's complexity makes it practically impossible to model its chemistry exactly, so an appropriate 3-component toluene reference fuel (TRF) surrogate comprised of toluene, *n*-heptane and iso-octane, formulated in (Agbro et al., 2017), is used to represent gasoline in this work. The detailed blended chemical kinetic model of *n*-butanol and TRF, developed in (Agbro et al., 2017) was evaluated using linear sensitivity method employing the brute force approach. Here, global uncertainty and sensitivity methods described fully in (Tomlin, 2013, Tomlin, 2006) is employed to provide further insight into the underlying chemistry mainly influencing the observed ignition delay behavior of the gasoline/butanol blends. While the linear sensitivity approach serves to highlight the important reactions driving the influence of *n*-butanol on ignition delay times when blended with gasoline at low temperatures, the global uncertainty and sensitivity analysis is carried out here to explore non-linear effects across the entire range of the input parameter space and the impact of the inherent uncertainties in the combined gasoline and *n*-butanol scheme on the predicted ignition

delay times of *n*-butanol, TRF and TRF-*n*-butanol blend. This is aimed at providing useful information for kinetic studies that will improve model robustness. Sensitivity indices calculated within the global analysis, based on the application of a HDMR metamodel(Ziehn and Tomlin, 2009, Tomlin and Turanyi, 2013) further helps to appropriately identify the key reaction rates that mostly influence (or determine) the predicted target uncertainties and this is quite useful where a nonlinear relationship exist between the sampled rates and predicted ignition delays within particular region of the input space. The global approach also allows us to understand how the interaction between various parameters in the kinetic model affect the predicted target output. Such information is critical to gain better insight into the complex chemistry behind the auto-ignition process for improved quantification of the chemical kinetic model.

Table 1: Properties of gasoline, *n*-butanol, ethanol and methanol (Wigg, 2011)

Fuel	Gasoline regular (PON 87)	*n*-Butanol	Ethanol	Methanol
Chemical formula	$CH_{1.87}$	C_4H_9OH	C_2H_5OH	CH_3OH
Specific gravity	0.7430	0.8097	0.7894	0.7913
Lower Heating Value (MJ/kg)	42.9	32.01	26.83	20.08
Stoichiometric air-fuel ratio (kg_{air}/kg_{fuel})	14.51	11.12	8.94	6.43
Energy density (MJ/l)	31.9	25.9	21.2	15.9
Latent heat of vaporisation (at boiling point) (kJ/kg)	349	584	838	1098
Octane number (RON+MON)/2	87	86	100	99

2.0 METHODOLOGY

2.1 Chemical kinetic scheme

While a few detailed and reduced mechanisms of gasoline oxidation involving primary reference fuels (PRFs), toluene reference fuels (TRFs) and more complex surrogates currently exist in the literature (Mehl et al., 2011, Tanaka et al., 2003, Glaude et al., 2002, Westbrook et al., 1988, Andrae et al., 2007, Andrae, 2008, Naik et al., 2005), the only combined oxidation mechanism for gasoline (toluene, n-heptane, iso-octane mixture)/*n*-butanol blends available at the time of this study was the detailed scheme presented in (Agbro et al., 2017). For the purpose of this study, a reduced version of the TRF/*n*-butanol blended mechanism, developed from the detailed scheme for use in the context of simulating autoignition and knock in the engine was adopted. The detailed scheme contains 1944 species and 8231 elementary reactions while the reduced scheme employed here is comprised of 527 species and 2644 reaction steps. More information on the detailed TRF/*n*-butanol blended mechanism can be found in (Agbro et al., 2017) while information on the reduced scheme can be found in (Agbro, 2017).The reduced TRF/*n*-butanol kinetic scheme, originally in Chemkin format, was first converted to Cantera input format (.cti file including the thermodynamic data) using the Cantera 2.1.2 ck2ti.py subroutine before it was used in the simulations.

2.2 Simulations and uncertainty/sensitivity analysis

Ignition delay times measured in the Leeds RCM and presented in (Agbro et al., 2017), were simulated in this work using the open source Cantera software toolbox (version 2.1.2) (Goodwin, 2013) by running homogeneous variable volume history simulations accounting for heat loss in the experiments. The volume profiles of the RCM employed in the simulations were determined from the measured pressure trace of the non-reactive experiment using isentropic core relations and a temperature-dependent mixture specific heat ratio (Weber and Sung, 2013).
A screening process utilizing local sensitivity method and based on the Brute-force method, was first applied to the *n*-butanol/TRF kinetic scheme in order to reduce the number of input parameters involved in the global uncertainty/sensitivity analysis since only a few key reactions are likely to greatly influence the accuracy of the predicted targets. The screening technique and the results of this local approach are presented in (Agbro et al., 2017). In the work of Agbro (Agbro et al., 2017), Brute-force sensitivity analyses were conducted at 20 bar and various temperature conditions using the closed homogeneous batch reactor module in CHEMKIN PRO (Reaction Design, 2011) and constant volume simulations. A total of 32 reactions (see appendix A) were captured in the linear sensitivity analyses reported in (Agbro et al., 2017) and these set of reactions are here further analyzed using global uncertainty and sensitivity methods.
The global sampling technique described in detail in (Tomlin, 2013), was applied in the simulations in order to quantify the error bars of the ignition delays predicted by the TRF/*n*-butanol scheme while incorporating the uncertainties of the input rate parameters in the simulations. Uncertainty factors obtained from either both published evaluations (Baulch et al., 2005, Baulch et al., 1994, Baulch et al., 1992, Tsang, 1992, Tsang and Hampson, 1986) and experimental data or from estimates made in the absence of sufficient data were assigned to the 32 most important reactions screened out across the three fuel mixture using the Brute-force method. An uncertainty factor of 10 was assigned to the reaction rates in the cases where there were no data on the uncertainty range of the reaction rate. The list of the uncertainty factors assigned to the set of reactions considered in the global analysis of the TRF/*n*-butanol mechanism can be found in Appendix A. In addition, a variance-based global sensitivity analysis using HDMR (Ziehn and Tomlin, 2009) is carried out to understand and rank the parameters responsible for the predicted uncertainties. Global sensitivity plots representing the first-order and second-order response between sampled input rates and predicted output are presented and discussed in the result section to explore and demonstrate how the choice of a parameter in the scheme impacts on the predicted ignition delay uncertainties.

3.0 RESULTS AND DISCUSSIONS

3.1 Global uncertainty and sensitivity analysis based on predicted TRF ignition delays

Figure 1 presents the uncertainty plot for predicted TRF ignition delays at ϕ = 1 and temperature range of 679 - 858 K using the blend mechanism while accounting for the effect of uncertainties in the input rate parameters. The uncertainty factors adopted in the uncertainty analysis of the TRF/*n*-butanol blended mechanism are given in

Appendix A. In Figure 1, the boxes represent 25th and 75th percentiles while whiskers represent 5th and 95th percentiles. The blue dashed line represents model simulation with nominal parameter values while the large crosses and horizontal lines represent the mean and median of the predicted output from the 256 simulations respectively. Figure 1 shows that the error bars currently existing within the TRF system are quite large rising above an order of magnitude in the negative temperature coefficient (NTC) region where the model performance is weakest. However, the experimental data points overlap fairly well with the predicted error bars indicating that reasonable values of uncertainty factors have been adopted for the key rates in the blend scheme. This also indicate that the model is reasonably sound in terms of its structure or mechanistic framework despite the parametric deficiency. Within the NTC region, the measured ignition delays are in closest agreement with the 25th percentile of the predicted distribution suggesting that some key input parameters would need to be fairly close to the limit of their input uncertainty range in order to improve the level of agreement of the model with experimental data.

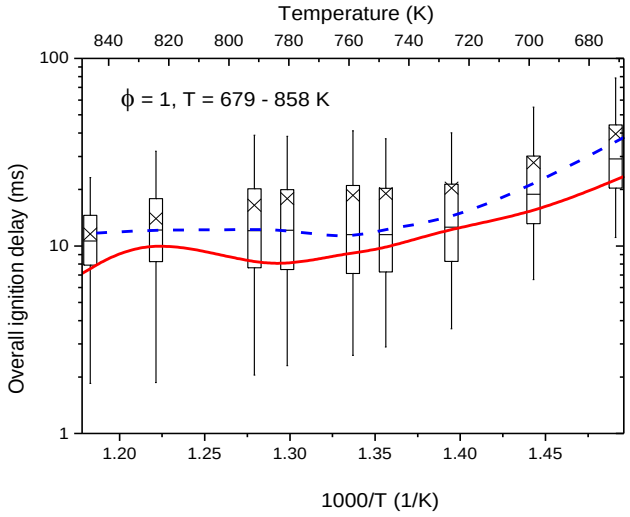

Figure 1. Comparison of predicted TRF ignition delays with experimental data (red line) obtained in Agbro et al.

Figure 2 highlights the first–order global sensitivity indices computed for ignition delay times using the variance based HDMR method for three representative temperature conditions at ϕ = 1 and P = 20 bar. This approach provides a ranking of each input parameter in terms of their contribution to the overall output variance. Figure 2 shows that at the lower temperature (i.e. 679 K), a total of seven reactions involving fuel + OH contribute to over 80% of the predicted error bars. The most dominant reaction at lower temperatures is that of OH + toluene expressed as the reverse (CH_3 + C_6H_5OH = $C_6H_5CH_3$ + OH) with its contribution being about 30 % of the overall predicted uncertainties. This is somewhat surprising since a recent theoretical study by Seta et al. (Seta et al., 2006) suggested this to be significantly slower than the hydrogen abstraction route via OH. Further investigation performed in this study to understand why the H abstraction is not the dominant route is presented in section 3.4. Hydrogen abstraction reactions by OH from the α, β and γ sites of iso-octane and *n*-heptane were also found to play a significant role in agreement with the local sensitivity study presented in (Agbro et al., 2017). At higher temperatures, the contribution from the

reaction $CH_3 + C_6H_5OH = C_6H_5CH_3 + OH$ diminishes considerably (disappearing at T = 858 K) with the H abstraction reaction from the γ site for iso-octane via OH becoming far more dominant. The main first-order global sensitivities shown in Figure 2 indicates that the alkyl + HO_2 reactions for toluene are also quite important for the predicted TRF ignition delays at high temperatures. Also, for toluene a growing importance is observed for the isomerisation reaction from RO_2 to QOOH as the temperature increases. The white portion in Figure 2 represents the contribution from reactions that are not displayed in the legend or the combined effect from higher order terms.

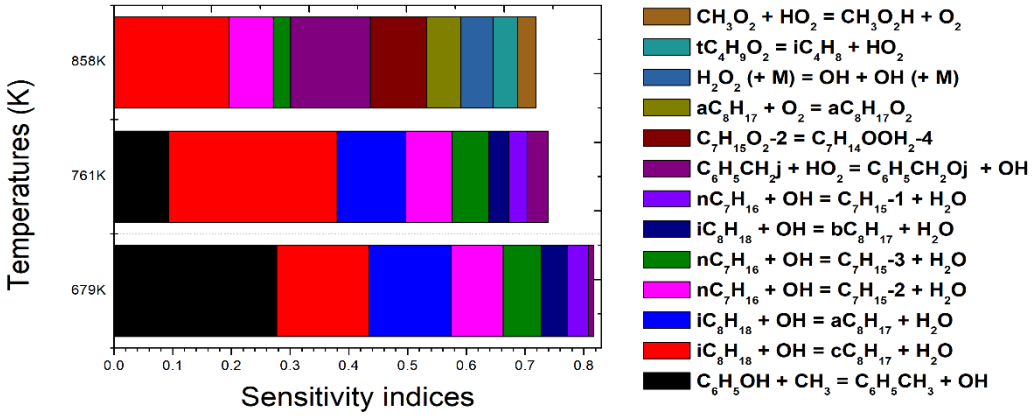

Figure 2. Main first-order sensitivity indices for simulated ignition delays of TRF at ϕ =1 and P = 20 bar with respect to the key reaction rates at selected temperatures and pressures.

The analysis of the first-order component functions plots further helps to explore the shape of the relationship between the input parameters and the target output. The component function plots shown in Figure 3 highlights the individual response of the predicted targets to changes in the A-factor for these reactions. The data points in these figures represent the individual responses from the quasi random sample whereas the line (component function) illustrates the individual effect of the chosen parameter. In each case shown, the middle point on the x-axis (0.5) represents the current nominal value of the A-factor used in the model. The first-order component plots (Figure 3) show that at T = 679 K, a nonlinear relationship exists between the target output and input rates across a large portion of the input space for all three most important reactions dominating the predicted uncertainties. Decreasing the rate of the phenol route ($CH_3 + C_6H_5OH = C_6H_5CH_3 + OH$) (Figure 3a) would likely improve the agreement with the experimental data at low temperature due to the attendant increase in reactivity while reducing the rate of the H abstraction reaction for iso-octane from the γ site (Figure 3c), would have no significant effect on the predicted uncertainties as the effect saturates in the lower part of the input space. On the other hand, increasing the rate of the abstraction reaction from the α site for iso-octane (Figure 3b) could potentially lead to an increase in reactivity of the TRF system at low temperature and better agreement with experiment but this is still dependent on the influence of second-order and higher order interactions. One interesting thing we observe in Figure 3b is that the influence of the uncertainties from all other reactions reduces considerably in the upper part of the input range as shown by the scatter which narrows down in this region and this would

suggest that some reasonable level of constraint is provided by the ignition delay measurements on this iso-octane H abstraction rate by OH.

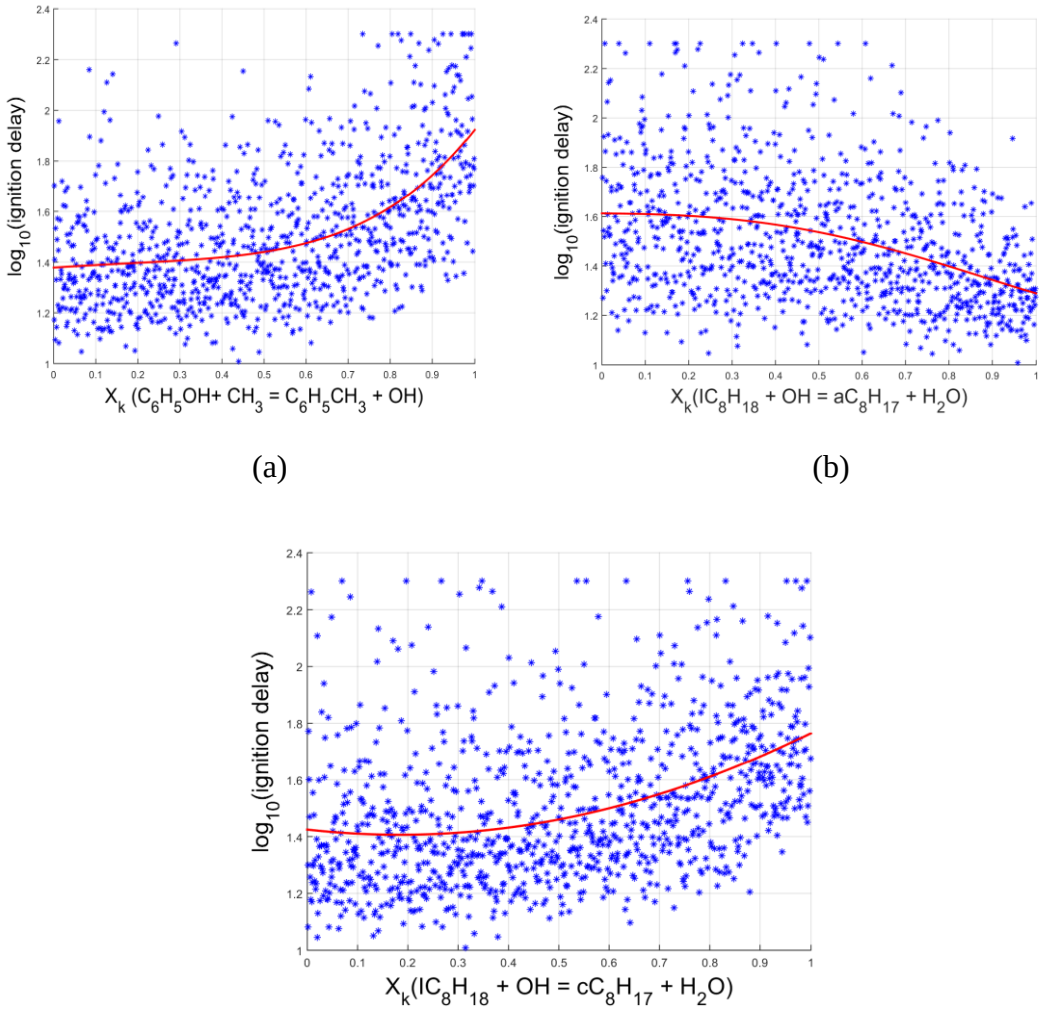

Figure 3. HDMR component functions (solid line) of simulated TRF ignition delays shown on-top of the scatter. P = 20 bar, ϕ = 1, T = 679 K. Sensitivity with respect to (a) CH3 + C_6H_5OH = $C_6H_5CH_3$ + OH (b) IC_8H_{18} + OH = aC_8H_{17} + H_2O (c) IC_8H_{18} + OH = cC_8H_{17} + H_2O.

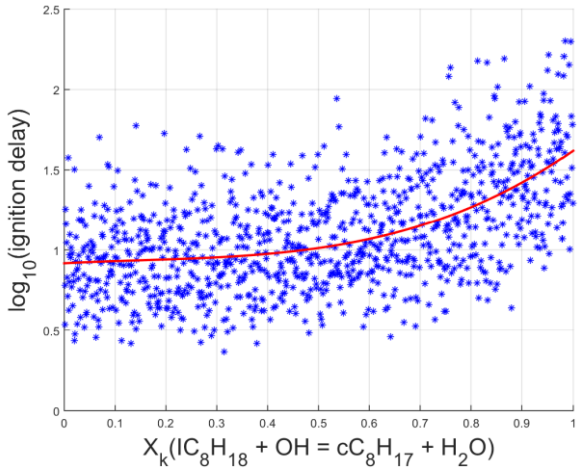

Figure 4. HDMR component functions (solid line) of simulated TRF ignition delays shown on-top of the scatter. P = 20 bar, ϕ = 1, T = 761 K. Sensitivity with respect to IC_8H_{18} + OH = cC_8H_{17} + H_2O.

Within the NTC region, specifically at T = 761K, the iso-octane H abstraction reaction by OH from the γ site, dominates the predicted uncertainties (Figure 2) with the reactions CH_3 + C_6H_5OH = $C_6H_5CH_3$ + OH, iC_8H_{18} + OH = aC_8H_{17} + H_2O and nC_7H_{16} + OH = C_7H_{15}-2 + H_2O also contributing to a smaller degree. However, looking at the functional relationship between the rate of this reaction IC_8H_{18} + OH = cC_8H_{17} + H_2O and the predicted ignition delays (Figure 4), no significant constraint is provided by the measured delays on this rate in the lower region of the input space where better agreement may be obtained as the slope of the first-order response is very close to zero in that region. On the other hand, a plot of the predicted log ignition delay against the scaled ratio of the log reaction rates for the iso-octane H abstraction reactions by OH from the α and γ site results in an almost linear relationship as shown in Figure 5. The computed sensitivity index of this branching fraction for iso-octane is 0.622 which is about three times the value of sensitivity for the individual reactions. Again, similar to what was observed for the *n*-butanol + OH system (Agbro and Tomlin, 2017), this demonstrates the importance of the relative rates of the hydrogen abstraction reactions of iso-octane from the different sites that lead to chain branching compared to the competing reaction channels that lead to chain propagation or termination, on the accurate prediction of the ignition delay times of TRF in the RCM. Therefore better constraint is provided by the measured ignition delay data on the branching ratio for iso-octane than on the individual abstraction rates via OH from the and γ site.

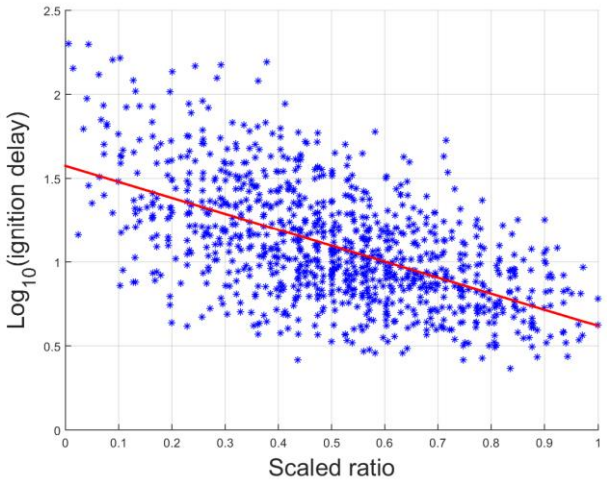

Figure 5. Scatter plot and HDMR component function for predicted log (ignition delay) of TRF against the scaled branching ratio for the two iso-octane main H abstraction reactions T = 761 K, ϕ = 1, P = 20 bar.

3.2 Global uncertainty and sensitivity analysis of predicted ignition delays based on the influence of n-butanol blending on gasoline

Figure 6 and Figure 7 show the calculated error bars for the simulated ignition delay times of TRF/*n*-butanol and neat *n*-butanol using the combined TRF and *n*-butanol scheme adopted in this study. In Figure 6 and Figure 7, the boxes represent 25th and 75th percentiles while whiskers represent 5th and 95th percentiles. The large crosses and horizontal lines represent the mean and median of the predicted output from the 256 simulations respectively.

Looking at Figure 6, we see that the predicted uncertainties for the TRF/*n*-butanol mixtures are largest (i.e. above an order of magnitude) in the temperature region 761 – 834 K where the discrepancy between the model's prediction and measured data is most pronounced. However, the experimental data falls well within the median (50th percentile) of the predicted ignition delay distribution. In contrast to the experimental data, at the lowest temperatures, the simulated ignition delay profiles for *n*-butanol fall close to the outliers far away from the median of the distribution. In the uncertainty analysis, at very low temperatures, certain combinations of the sampled input rates resulted in extremely long ignition delay times and such results were therefore truncated in order to reduce the required computational time. This explains why the simulated delay times at the nominal rate (blue line) are now shifted closer to the outliers of the distribution rather than the median of the distribution. This explanation is also true for the predicted TRF/*n*-butanol distribution shown in Figure 6 but in this case the effect is less pronounced compared to that of pure *n*-butanol due to the lower predicted ignition delay times of the blend. For *n*-butanol, the predicted uncertainties (Figure 7) are the largest and are over two orders of magnitude in the low temperature region where the models agreement with the measured data is also worse. The discussion in the next section is centred on the global HDMR analysis carried out in order to highlight the

most important reactions influencing the predicted *n*-butanol and TRF/*n*-butanol output distribution.

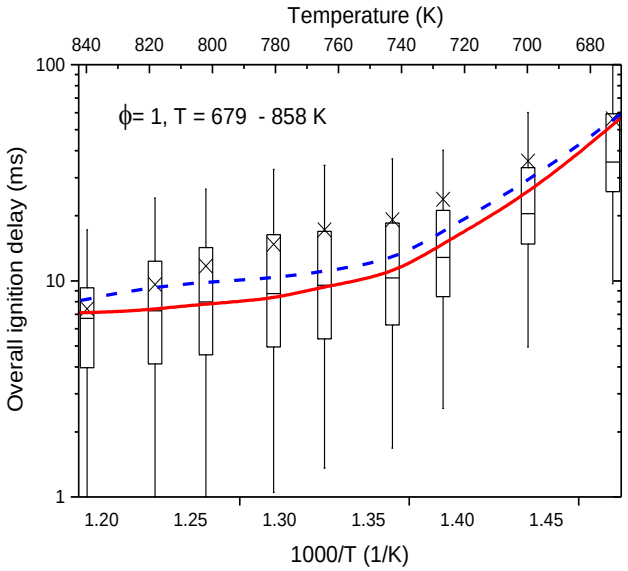

Figure 6. Comparison of predicted TRF/*n*-butanol ignition delays (blue) with experimental data (red) obtained in this study.

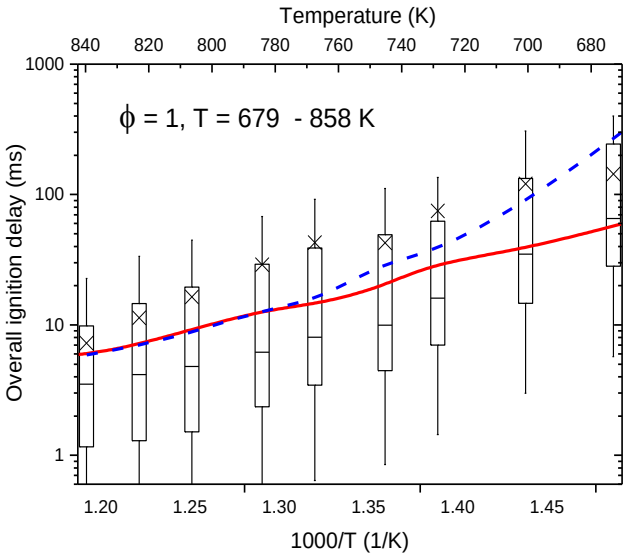

Figure 7. Comparison of predicted *n*-butanol ignition delays (blue) with experimental data obtained (red) in this study.

Figure 8 shows the first-order sensitivity indices calculated in the HDMR analysis for predicted *n*-butanol + TRF ignition delay times. At lower temperatures, the *n*-butanol + OH hydrogen abstraction reaction from the α site is found to be the most dominant reaction in terms of its contribution to the predicted uncertainties. Other key reactions contributing to the predicted uncertainties include $C_4H_8OH\text{-}1 + O_2 = C_4H_8OH\text{-}1O_2$, $IC_8H_{18} + OH = aC_8H_{17} + H_2O$ and $C_6H_5OH + CH_3 = C_6H_5CH_3 + OH$. As the temperature is increased to 858 K, the relative dominance of the *n*-butanol + OH abstraction reaction

from the α site becomes significantly smaller while that of abstraction from the γ site conversely increases with abstraction from the γ site dominating the predicted uncertainties at T = 858 K. The trend observed within the global sensitivity framework for the TRF/*n*-butanol system is similar to that obtained using the local sensitivity approach except that in the local sensitivity analysis, at T = 858 K, the reaction involving hydroperoxyl, leading to the formation of H_2O_2 (HO_2 + HO_2 = H_2O_2 + O_2) was slightly more dominant compared to the *n*-butanol + OH abstraction reaction from the γ site.

For the *n*-butanol system, the results of the HDMR analysis (Figure 9) show that at the lower temperature (i.e. T = 679 K), the chain branching pathway (alpha-hydroxybutyl + O_2) leading to the formation of the peroxy radical (RO_2) (γ -C_4H_8OH-1 + O_2 = C_4H_8OH-1O_2) is the most dominant reaction, being responsible for over 20 % of the predicted uncertainties. This was not the case for the local sensitivity analysis of *n*-butanol where the hydrogen abstraction from the γ site of the *n*-butanol + OH channel dominated the uncertainties in the predicted ignition delay times. In the *n*-butanol system, a smaller fraction of the overall uncertainties (about 10 % and 12 %) is also accounted for by the α and γ branching fractions of *n*-butanol + OH respectively. The slight difference between the most dominant reaction channel obtained in the local sensitivity analysis and that captured in the global sensitivity analysis can be attributed to the impact of the input uncertainty range adopted for the chain branching pathway relative to that of the H abstraction reaction from *n*-butanol by OH (see Appendix A for table of uncertainty range). The impact of the chain branching reaction however diminishes with increases in temperature while the contribution from *n*-butanol + OH abstraction reaction from the γ site, becomes more significant similar to the result obtained for the local sensitivity analysis. At high temperature, the H abstraction reaction from *n*-butanol by HO_2 leading to the formation of C_4H_8OH-1 and H_2O_2 is shown to be equally as important as the abstraction reaction from the γ site.

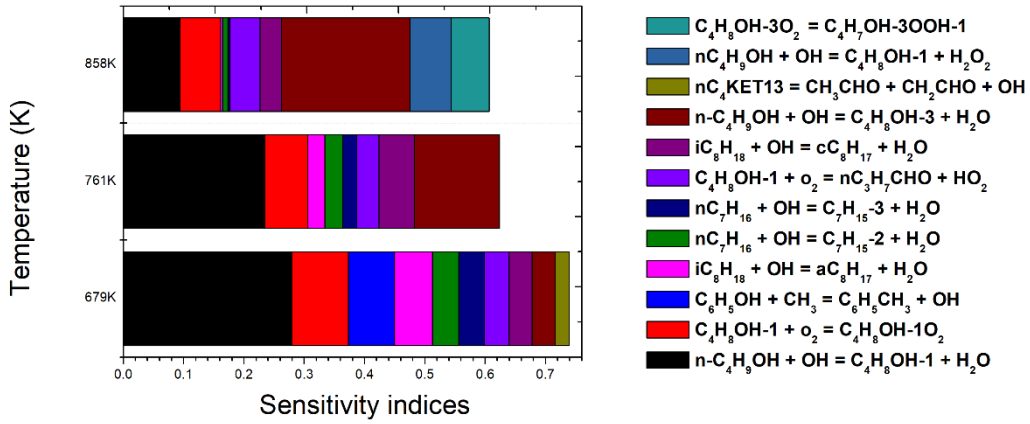

Figure 8. Main first-order sensitivity indices for simulated TRF/*n*-butanol ignition delays with respect to reaction rates at selected temperatures and pressures. The shading for each reaction is shown in the legend. P = 20 bar, ϕ = 1.

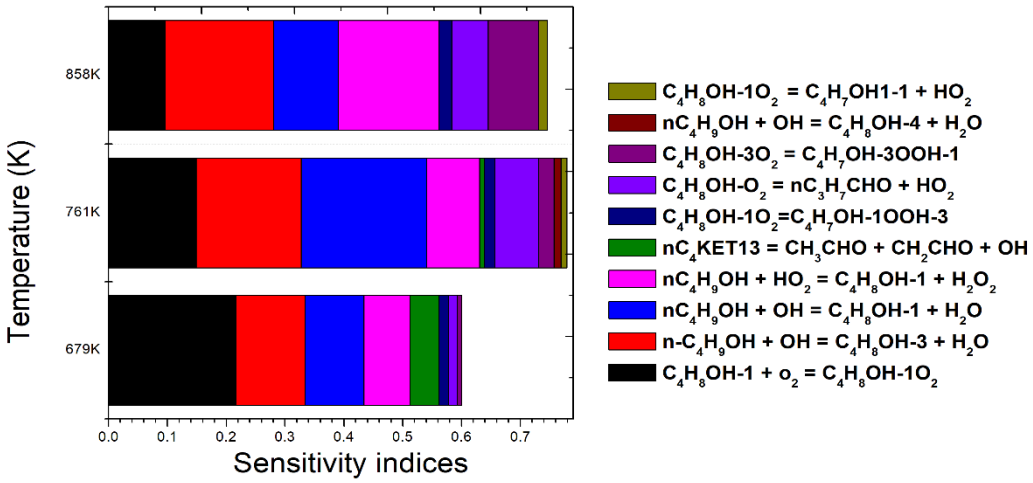

Figure 9. Main first-order sensitivity indices for simulated *n*-butanol ignition delays with respect to reaction rates at selected temperatures and pressures. The shading for each reaction is shown in the legend. P = 20 bar, ϕ = 1.

Based on the computed sensitivity indices from the HDMR analysis (Figure 8) it is clear that the branching fractions of *n*-butanol + OH (α and γ site) with global sensitivity indices of 0.234 and 0.142 respectively are important for the TRF/*n*-butanol system at 761 K as they account for about 40 % of the predicted output uncertainties in this region where the highest discrepancy occurred. Figure 10 presents the first-order component plots for these two abstraction reactions at T = 761 K with the scatter in the figure representing the impact of the uncertainties in the other parameters within the mechanism. The overall response of these two parameters to the predicted delays is nonlinear and the overall slopes are opposite to one another. While a reasonable level of constraint is provided in the individual rate of the two abstraction reactions by the measured data as indicated by the computed sensitivities, none of them solely dominates the predicted output uncertainties meaning that different combinations of these two rates could lead to different levels of improvement in terms of the agreement with the experimental data. The high temperature component plot for the TRF/*n*-butanol system (Figure 11) shows that a decrease in the γ abstraction rate of *n*-butanol + OH could potentially also lead to improvement in the model's prediction at high temperatures.

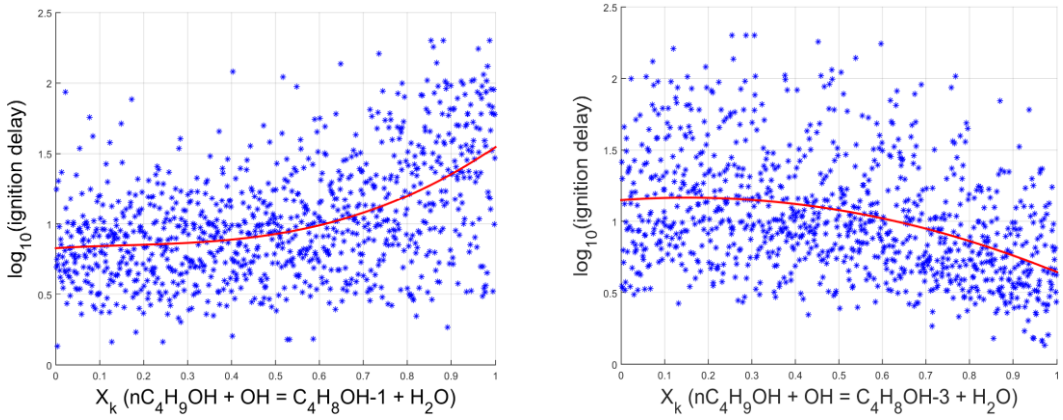

(a) (b)

Figure 10. Component function for TRF/*n*-butanol mixture at *T* = 761 K with respect to (a) *n*-C_4H_9OH + OH = C_4H_8OH-1 + H_2O (b) *n*-C_4H_9OH + OH = C_4H_8OH-3 + H_2O.

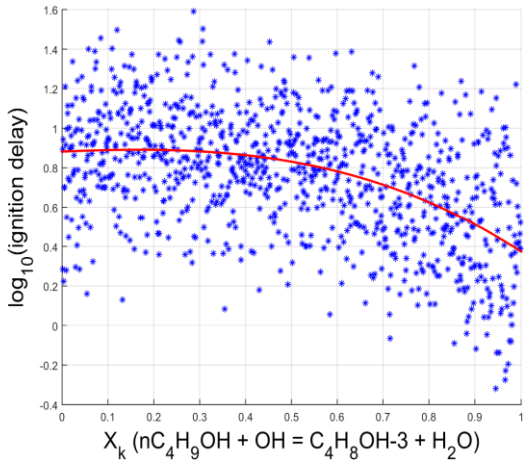

Figure 11. Component function for TRF/*n*-butanol mixture at *T* = 858 K with respect to *n*-C_4H_9OH + OH = C_4H_8OH-3+ H_2O.

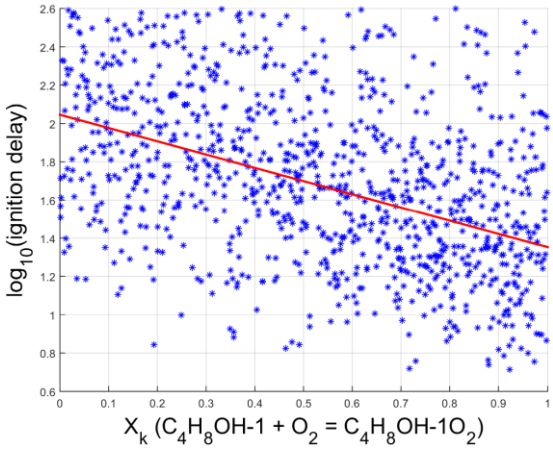

Figure 12. Component function for *n*-butanol mixture at 679 K with respect to C_4H_8OH-1 + O_2 = C_4H_8OH-1O_2.

Figure 12 shows that the predicted *n*-butanol ignition delays are well correlated to the O_2 addition pathway and a large increase in this rate could potentially lead to a considerable decrease in the predicted *n*-butanol delays at lower temperatures. The large scatter however indicates that other reaction pathways such as the competing termination step leading to the formation of HO_2 (C_4H_8OH-1 + O_2 = n-C_3H_7CHO + HO_2), could become more significant as the rate of this reaction is increased.

3.4 Analysis of toluene + OH system

3.4.1 Comparison of Arrhenius parameters

The results of the local sensitivity analysis reported in (Agbro et al., 2017) and the global sensitivity analysis described in section 3.3 for predicted ignition delay times for TRF using the combined TRF/*n*-butanol mechanism, showed a strong sensitivity to the reaction toluene + OH = phenol + CH_3 rather than the hydrogen abstraction channels by OH (toluene + OH = $C_6H_4CH_3$ + H_2O). This was however not expected as a recent study by Seta et al. (Seta et al., 2006) on the reaction of OH radicals with benzene and toluene suggested that the hydrogen abstraction route (toluene + OH = $C_6H_4CH_3$ + H_2O) is significantly faster than the toluene + OH route leading to the formation of phenol. Figure 13 shows Arrhenius plots in which the temperature dependence of the forward rates of the toluene + OH = $C_6H_4CH_3$ + H_2O and toluene + OH = phenol + CH_3 reaction pathways obtained from the study of Seta (Seta et al., 2006), are compared. From Figure 13, it is clear the OH abstraction routes could be over ten times faster than the phenol route across the temperature range.

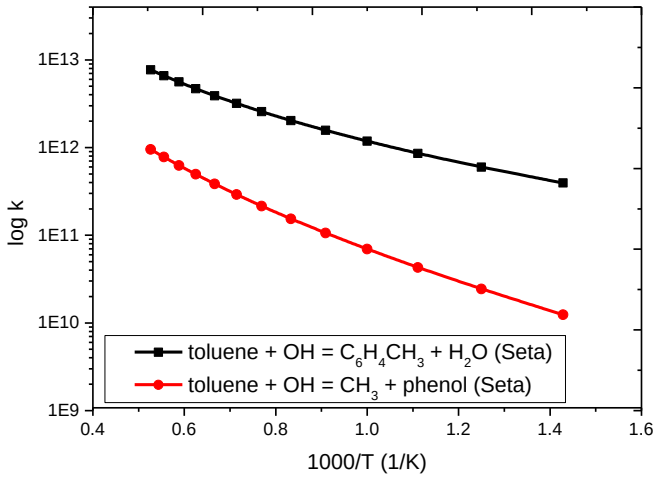

Figure 13. Comparison of the forward rates of toluene H abstraction route (toluene + OH) and the phenol route from a recent study of Seta (Seta et al., 2006).

In order to understand why the H abstraction channel is not the dominant route, a critical investigation of the sources of the data for the current parametrisation of the two toluene + OH routes in the available version of the LLNL TRF mechanism was therefore carried out. It was found in the course of the investigation that the current parametrisation of the H abstraction route (toluene + OH = $C_6H_4CH_3$ + H_2O) in the LLNL TRF mechanism, is based on the recent data from the theoretical study of Seta. The H abstraction reactions in the LLNL scheme were updated from the paper of Seta

(Seta et al., 2006), but for some reason which is not clear as at the time of this study, it appears that the toluene + OH channel leading to the formation of phenol (toluene + OH = phenol + CH_3) was not updated from the same source. In the update of Mehl (Mehl et al., 2011), all attacks on the toluene ring by OH including the reaction toluene + OH = $C_6H_4CH_3$ + H_2O in the mechanism were taken to be the same with the ones estimated by Seta (Seta et al., 2006) for benzene.

In order to test the impact of the differences between the rate parameterisation of the reversed form of the phenol route (phenol + CH_3 = toluene + OH) which is currently in the TRF/*n*-butanol mechanism and that derived from the study of Seta (Seta et al., 2006), on the predicted ignition delays, a new set of reaction rates was first of all computed for the reversed form of the aforementioned reaction using the forward rate data obtained from the paper of Seta (Seta et al., 2006). The method employed for the computation of the reversed reaction rates is described briefly in the following section.

3.4.2 Calculation of reversed rate based on data of Seta

In the Cantera chemical kinetic tool (version 2.1.2) (Goodwin, 2013), the temperature dependence of the forward rate constants k_f follows the Arrhenius expression given by:

$$k_f = A_f T^{n_f} \exp\left(-E_f/RT\right) \tag{1}$$

whereA_f is the A -factor (pre-exponential factor), n_f is the temperature exponent, E_f is the activation energy, T is the absolute temperature and R is the universal gas constant.

The equilibrium constant k_{eq}relates the forward rate to the reversed rate and can be calculated from standard thermodynamic properties using the relationship:

$$k_{eq} = \exp\left(\Delta S^0/_R\right) * \exp\left(-\Delta H^0/_{RT}\right) \tag{2}$$

where ΔS^0 and ΔH^0 are respectively the standard molar entropy and enthalpy changes of the reaction computed from the respective standard molar entropies S^0 and enthalpies $H^0$of the species taking part in the reaction and R is the gas constant.

Also, the equilibrium constant is given by,

$$\frac{k_f}{k_r} = k_{eq} \tag{3}$$

By using Equation 2 and 3, the reversed rates of any reaction can be calculated if the forward rates are known. The temperature-dependent reversed rates for the phenol route were determined using the value of the forward rates of the reaction given in the paper of Seta (Seta et al., 2006) alongside the equilibrium rate constants estimated using the NASA polynomials in the thermodynamic data of the TRF/*n*-butanol mechanism for the involved species. In the thermodynamic data seven polynomial coefficients are specified for the low temperature range typically from 300 K to 1000 K and another seven for the high temperature range usually from above 1000 K up to 5000 K. The NASA polynomials for standard molar heat capacity at constant pressure ${C_p}^\theta$, enthalpy H^θ, and entropy S^θ, take the form:

$$\frac{{C_p}^{\theta}}{\bar{R}} = a_1 + a_2T + a_3T^2 + a_4T^3 + a_5T^4 \quad (4)$$

$$\frac{H^{\theta}}{\bar{R}T} = a_1 + \frac{a_2}{2}T + \frac{a_3}{3}T^2 + \frac{a_4}{4}T^3 + \frac{a_5}{5}T^4 + \frac{a_6}{T} \quad (5)$$

$$\frac{S^{\theta}}{\bar{R}} = a_1 \ln T + a_2T + \frac{a_3}{2}T^2 + \frac{a_4}{3}T^3 + \frac{a_5}{4}T^4 + a_1 \quad (6)$$

Where *T* is temperature in Kelvin, $\bar{R}$ is the universal gas constant in kJ/kmol and the a_n parameters are the NASA polynomial coefficients.

Table 2 gives the values of the equilibrium constant and reversed rates calculated across the temperature range 700 -1900 K using Equations (1-6).

Table 2. Calculated equilibrium constant and reversed rates

Temperature (K)	k_f(T)[c]	$k_{eq}(T)$	$k_r(T)$
700	1.24×10^{10}	6.94×10^{2}	1.79×10^{7}
800	2.43×10^{10}	3.53×10^{2}	6.90×10^{7}
900	4.28×10^{10}	2.09×10^{2}	2.05×10^{8}
1000	6.95×10^{10}	1.38×10^{2}	5.02×10^{8}
1100	1.06×10^{11}	9.85×10^{1}	1.08×10^{9}
1200	1.54×10^{11}	7.42×10^{1}	2.07×10^{9}
1300	2.15×10^{11}	5.83×10^{1}	3.69×10^{9}
1400	2.91×10^{11}	4.73×10^{1}	6.16×10^{9}
1500	3.84×10^{11}	3.95×10^{1}	9.72×10^{9}
1600	4.95×10^{11}	3.37×10^{1}	1.47×10^{10}
1700	6.26×10^{11}	2.93×10^{1}	2.14×10^{10}
1800	7.78×10^{11}	2.57×10^{1}	3.02×10^{10}
1900	9.53×10^{11}	2.27×10^{1}	4.20×10^{10}

[c] Values obtained from the paper of Seta (Seta et al., 2006)

The associated reversed rate parameters required in the CANTERA input file for the simulations, such as the temperature exponent *n*, frequency factor *A* and activation energy *E* were further estimated using a least square fit to the reversed rate data.

As presented in Figure 14, a comparison of the rates of the reversed form of the phenol route (toluene + OH = phenol + CH_3) captured in the LLNL mechanism with those estimated from the data of Seta shows a significant difference in their temperature dependence. Although both rate constant parameterisation are closely matched at high temperature, the disparity is quite large at lower temperatures.

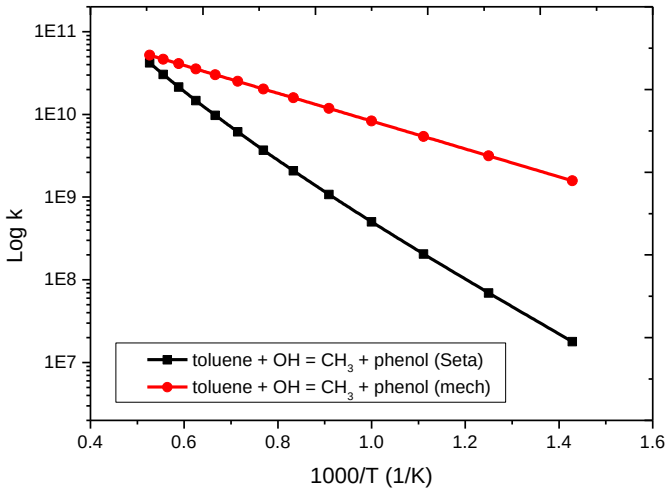

Figure 14. Comparison of the reversed rates of the phenol route (toluene + OH = phenol + CH_3) captured in the LLNL mechanism with those estimated from the data of Seta (Seta et al., 2006).

3.4.3 Impact of update on reaction mechanism based on new data

The rate of the phenol route in the mechanism was finally updated to that in the paper of Seta and variable volume ignition delay simulations were repeated based on the new set of data.

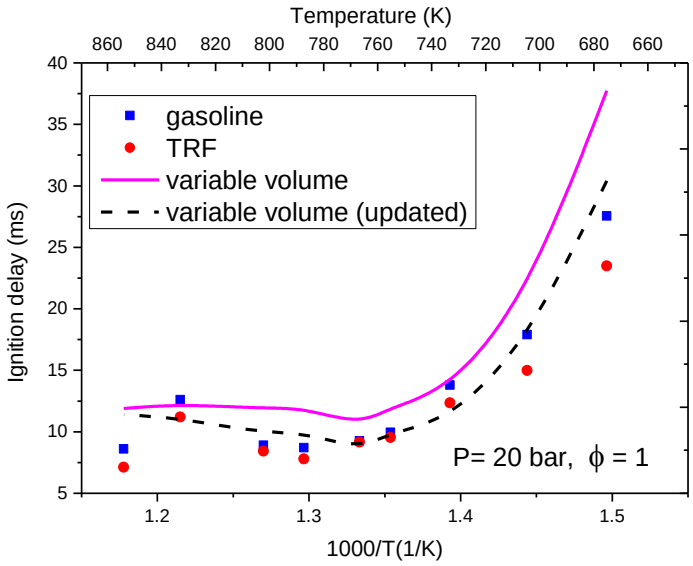

Figure 15. Ignition delay simulations showing how the updated mechanism compares with original LLNL data, TRF mixtures at P = 20 bar, ϕ = 1.

Figure 15 shows the result of the predicted TRF ignition delays based on the updated mechanism. Interestingly, as shown in Figure 15, the updated mechanism gives a better agreement with the experimentally measured ignition delays of TRF at P =20 bar under stoichiometric conditions. Also, we see that the NTC region is now predicted to a higher

level of accuracy and this is important for accurate prediction of autoignition and knock in practical engines. The update also leads to a reasonable improvement in the predicted ignition delays of the TRF, *n*-butanol blend (Figure 16) mainly within the lower to intermediate temperature region.

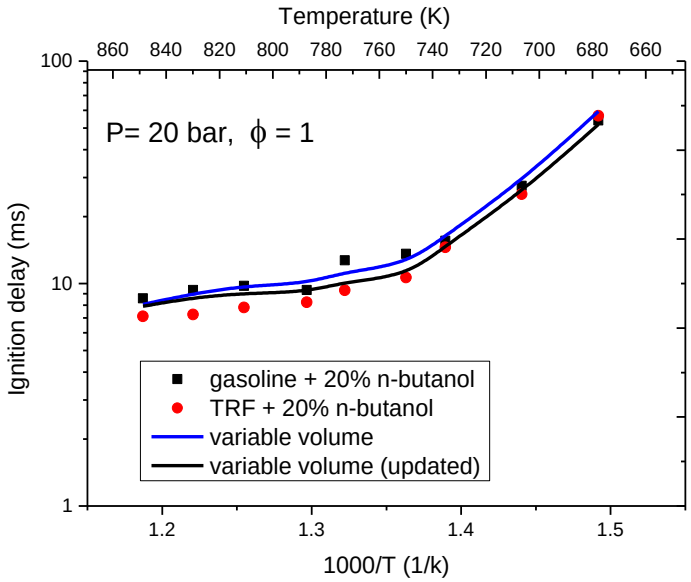

Figure 16. Ignition delay simulations showing how the updated mechanism compares with original LLNL data, TRF, *n*-butanol blend at P = 20 bar, ϕ = 1.

Furthermore, local sensitivity analysis was repeated for the TRF mixture using the updated scheme to see if the importance of this channel will now be replaced by the H abstraction route. The result of local sensitivity analysis based on the updated mechanism is presented in Figure 17 for fifteen (15) of the most sensitive reactions. As expected the toluene + OH hydrogen abstraction route is now captured as one of the most important (dominant) reactions for low temperature ignition delay prediction of TRF mixtures while the phenol route is shown to be relatively unimportant as it is not among the set of reactions identified in the sensitivity analysis. Interestingly, this is in agreement with the analysis of the component plot presented in Figure 3a (section 3.1) where the sensitivity of the phenol route given by the gradient of the curve is shown to be quite low at the lower end of the adopted input range.

It is also worth pointing out that based on the update, the iso-octane chemistry, specifically the iso-octane + OH hydrogen abstraction reaction from the γ site (Figure 17) now dominates the predicted ignition delays of TRF. Also the alkyl + HO_2 route for toluene which was prominent at higher temperatures in the local sensitivity result based on the original TRF/*n*-butanol mechanism has now disappeared.

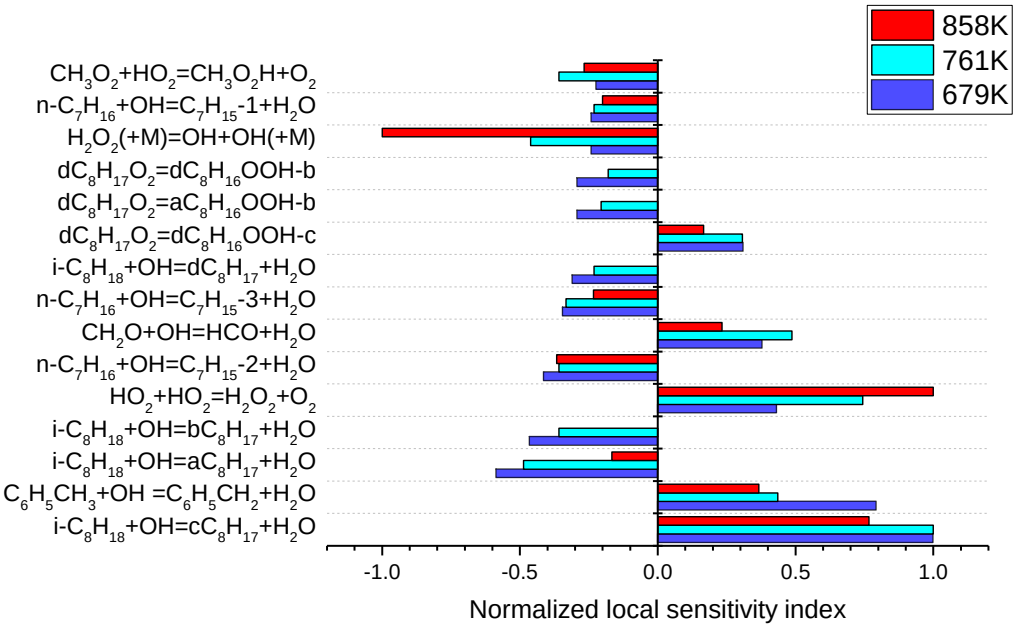

Figure 17. Brute-force local sensitivity result based on updated mechanism for TRF mixtures at P = 20 bar, ϕ = 1.

4.0 CONCLUSIONS

A recently developed reduced chemical kinetic mechanism describing the low temperature oxidation of n-butanol, gasoline and a gasoline/n-butanol blend was investigated using both global uncertainty and sensitivity methods with ignition delays as the predicted output for the temperature range 678 - 858 K, and an equivalence ratio of 1 at 20 bar. The work highlights and elucidates on the most important input parameters influencing the predictive output uncertainties in the chemical kinetic models when incorporating the effects of uncertainties in forward rate constants within a global sampling approach. For TRF, a total of seven reactions involving fuel + OH were identified as contributing to over 80% of the predicted error bars. The dominant reaction at lower temperatures is that of OH + toluene expressed as the reverse (CH_3 + C_6H_5OH = $C_6H_5CH_3$ + OH) but an update on the mechanism based on recent data from the study of Seta resulted in the toluene + OH channel becoming the most dominant reaction as expected. At higher temperatures, the contribution from the reaction CH_3 + C_6H_5OH = $C_6H_5CH_3$ + OH diminishes considerably (disappearing at 858 K) while the H abstraction reaction from the γ site via OH for iso-octane becomes far more dominant. The work showed that the hydrogen abstraction reactions by OH from n-butanol are the most important reactions in predicting the effect of *n*-butanol blending on gasoline particularly at the low temperature but these rates are still currently not well known and hence the large discrepancies currently existing in the models prediction in the low temperature region. For predicted *n*-butanol ignition delay times, the chain branching pathway (α-hydroxybutyl + O_2) leading to the formation of the peroxy radical (RO_2) (α-C_4H_8OH-1 + O_2 = C_4H_8OH-1O_2) is the most dominant, being responsible for over 20 percent of the predicted uncertainties. For both the n-butanol and TRF/n-butanol system, the contribution from *n*-butanol + OH abstraction reaction from the γ site, is the most significant at higher temperatures (i.e. 858K).

The global sensitivity plots representing the first-order and second-order response between sampled input rates and predicted output were also discussed to explore and illustrate how the choice of a parameterization in the scheme impacts on the predicted output uncertainties. First-order functional plots for TRF indicate that modifications to the rate of fuel + OH for toluene and that of H abstraction for iso-octane from the γ site are unlikely to improve the level of agreement with the experimental data at lower temperatures, but increasing the rate of the abstraction reaction from the α site for iso-octane could lead to a decrease in reactivity and better agreement. This is however, dependent on the influence of second-order and higher-order interactions. Within the NTC region where the iso-octane H abstraction reaction by OH from the γ site dominates, better constraint is provided by the measured ignition delay data on the rate of the branching ratio for iso-octane than on the overall or individual abstraction rate for the α and γ site. For TRF + n-butanol, the overall response for the two most dominant n-butanol + OH abstraction rates (α and γ site) to the predicted delays is nonlinear and opposite to one another. While a reasonable level of constraint is provided in the individual rate of these two abstraction reactions by the measured data, as indicated by the computed sensitivities, none of them solely dominants the predicted output uncertainties.

For predicted n-butanol + TRF ignition delay times, the n-butanol + OH hydrogen abstraction reaction from the α site is found to be the most dominant in terms of its contribution to the predicted uncertainties, despite the low blending ratio of butanol at 20%, while.

5.0 ACKNOWLEDGEMENTS

The author would like to thank the Tertiary Education Trust Fund (TETFUND), Nigeria, for providing funding for this research. My sincere appreciation also goes to Professor Alison Tomlin for her guidance and most importantly for the helpful discussions.

6.0 REFERENCES

Agarwal, A. K. 2007. Biofuels (alcohols and biodiesel) applications as fuels for internal combustion engines. *Progress in energy and combustion science,* 33**,** 233-271.

Agbro, E. 2017. *Experimental and chemical kinetic modelling study on the combustion of alternative fuels in fundamental systems and practical engines.* PhD, The University of Leeds.

Agbro, E. & Tomlin, A. S. 2017. Low temperature oxidation of n-butanol: Key uncertainties and constraints in kinetics. *Fuel,* 207**,** 776-789.

Agbro, E., Tomlin, A. S., Lawes, M., Park, S. & Sarathy, S. M. 2017. The influence of n-butanol blending on the ignition delay times of gasoline and its surrogate at high pressures. *Fuel,* 187**,** 211-219.

Andrae, J. C. G. 2008. Development of a detailed kinetic model for gasoline surrogate fuels. *Fuel,* 87**,** 2013-2022.

Andrae, J. C. G., Björnbom, P., Cracknell, R. F. & Kalghatgi, G. T. 2007. Autoignition of toluene reference fuels at high pressures modeled with detailed chemical kinetics. *Combustion and Flame,* 149**,** 2-24.

Baulch, D. L. 1997. Kinetic Databases. *In:* Pilling, M. J. (ed.) *Comprehensive Chemical Kinetics: Low Temperature Combustion and Auto-ignition.* Elservier.

Baulch, D. L., Bowman, C. T., Cobos, C. J., Cox, R. A., Just, T. H., Kerr, J. A., Pilling, M. J., Stocker, D., Troe, J., Tsang, W., Walker, R. W. & Warnatz, J. 2005. Evaluated kinetic data for combustion modeling: supplement II. *Journal of Physical and Chemical Reference Data,* 34**,** 757-1397.

Baulch, D. L., Cobos, C. J., Cox, R. A., Esser, C., Frank, P., Just, T., Kerr, J. A., Pilling, M. J., Troe, J., Walker, R. W. & Warnatz, J. 1992. Evaluated Kinetic Data for Combustion Modelling. *Journal of Physical and Chemical Reference Data,* 21**,** 411-734.

Baulch, D. L., Cobos, C. J., Cox, R. A., Frank, J. H., Hayman, G., Just, T. H., Kerr, J. A., Murrels, T., Pilling, M. J.; Troe, J., Walker, B. F. & Warnatz, J. 1994. Summary table of evaluated kinetic data for combustion modeling: Supplement 1. *Combustion and Flame***,** 59-79.

Dernotte, J., Mounaim-rousselle, C., Halter, F. & Seers, P. 2009. Evaluation of butanol–gasoline blends in a port fuel-injection, spark-ignition engine. *Oil & Gas Science and Technology–Revue de l'Institut Français du Pétrole,* 65**,** 345-351.

Glaude, P. A., Conraud, V., Fournet, R., Battin-leclerc, F., Côme, G. M., Scacchi, G., Dagaut, P. & Cathonnet, M. 2002. Modeling the Oxidation of Mixtures of Primary Reference Automobile Fuels. *Energy & Fuels,* 16**,** 1186-1195.

Goodwin, D. M., N; Moffat, H; Speth, R 2013. *CANTERA: an object-oriented software toolit for chemical kinetics, thermodynamics, and transport processes,* https://code.google.com/p/cantera.

Mehl, M., Pitz, W. J., Westbrook, C. K. & Curran, H. J. 2011. Kinetic modeling of gasoline surrogate components and mixtures under engine conditions. *Proceedings of the Combustion Institute,* 33**,** 193-200.

Naik, C. V., Pitz, W. J., Westbrook, C. K., Sjöberg, M., Dec, J. E., Orme, J., Curran, H. J. & Simmie, J. M. 2005. Detailed Chemical Kinetic Modeling of Surrogate Fuels for Gasoline and Application to an HCCI Engine. SAE International.

Reaction Design 2011. *Chemkin-pro,* San Diego.

Sarathy, S. M., Oßwald, P., Hansen, N. & Kohse-höinghaus, K. 2014. Alcohol combustion chemistry. *Progress in Energy and Combustion Science,* 44**,** 40-102.

Seta, T., Nakajima, M. & Miyoshi, A. 2006. High-temperature reactions of OH radicals with benzene and toluene. *The Journal of Physical Chemistry A,* 110**,** 5081-5090.

Szwaja, S. & Naber, J. D. 2010. Combustion of n-butanol in a spark-ignition IC engine. *Fuel,* 89**,** 1573-1582.

Tanaka, S., Ayala, F. & Keck, J. C. 2003. A reduced chemical kinetic model for HCCI combustion of primary reference fuels in a rapid compression machine. *Combustion and Flame,* 133**,** 467-481.

Tomlin, A. S. 2006. The use of global uncertainty methods for the evaluation of combustion mechanisms. *Reliability Engineering & System Safety,* 91**,** 1219-1231.

Tomlin, A. S. 2013. The role of sensitivity and uncertainty analysis in combustion modelling. *Proceedings of the Combustion Institute,* 34**,** 159-176.

Tomlin, A. S. & Turanyi, T. 2013. Investigation and Improvement of Mechanism using Sensitivity Analysis and Optimization. *In:* Battin-leclerc, F., Simmie, J. M. & Blurock, E. (eds.) *Cleaner Combustion: Developing Detailed Chemical Kinetic Models.* London: Springer-Verlag.

Tsang, W. 1992. Chemical Kinetic Data Base for Propellant Combustion. II. Reactions Involving CN, NCO, and HNCO. *Journal of Physical and Chemical Reference Data,* 21**,** 753-791.

Tsang, W. & Hampson, R. F. 1986. Chemical Kinetic Data Base for Combustion Chemistry. Part I. Methane and Related Compounds. *Journal of Physical and Chemical Reference Data,* 15**,** 1087-1279.

Weber, B. W. & Sung, C.-J. 2013. Comparative Autoignition Trends in Butanol Isomers at Elevated Pressure. *Energy & Fuels,* 27**,** 1688-1698.

Westbrook, C. K., Warnatz, J. & Pitz, W. J. 1988. A detailed chemical kinetic reaction mechanism for the oxidation of iso-octane and n-heptane over an extended temperature range and its application to analysis of engine knock. *Symposium (International) on Combustion,* 22**,** 893-901.

Wigg, B. 2011. *A Study on Emission of Butanol using a Spark Ignition Engine and their Reduction Using Electrostatically Assisted Injection.* PhD, University of Ilinois, Urbana.

Ziehn, T. & Tomlin, A. 2009. GUI–HDMR–A software tool for global sensitivity analysis of complex models. *Environmental Modelling & Software,* 24**,** 775-785.

APPENDIX A

Reactions selected from local sensitivity analysis of TRF/*n*-butanol blended mechanism and assigned input uncertainty factors

Reaction	G_i	K max	K min	Source of uncertainty information
$HO_2 + HO_2 = H_2O_2 + O_2$	1.41			(Baulch et al., 2005)
H_2O_2 (+ M) = OH + OH (+M) (k_0,k_∞)	3.16			(Baulch et al., 2005)
$H_2O_2 + OH = H_2O + HO_2$	1.58			(Tsang, 1992)
$CH_2O + OH = HCO + H_2O$	2.24			(Baulch et al., 2005)
$CH_3O_2 + HO_2 = CH_3O_2H + O_2$	5.0			Estimated
$nC_3H_7O_2 = C_3H_6OOH1\text{-}3$	10.0			Estimated
$nC_4KET13 = CH_3CHO + CH_2CHO + OH$	10.0			Estimated
$tC_4H_9O_2 = iC_4H_8 + HO_2$	10.0			Estimated
$iC_8H_{18} + OH = aC_8H_{17} + H_2O$	7.94			Estimated
$iC_8H_{18} + OH = bC_8H_{17} + H_2O$	3.98			Estimated
$iC_8H_{18} + OH = cC_8H_{17} + H_2O$	7.94			Estimated
$aC_8H_{17} + O_2 = aC_8H_{17}O_2$	10.0			Estimated
$dC_8H_{17}O_2 = dC_8H_{16}OOH\text{-}b$	10.0			Estimated
$dC_8H_{17}O_2 = dC_8H_{16}OOH\text{-}c$	10.0			Estimated
$nC_7H_{16} + OH = C_7H_{15}\text{-}1 + + H_2O$	10.0			Estimated
$nC_7H_{16} + OH = C_7H_{15}\text{-}2 + + H_2O$	10.0			Estimated
$nC_7H_{16} + OH = C_7H_{15}\text{-}3 + + H_2O$	10.0			Estimated
$C_7H_{15}O_2\text{-}2 = C_7H_{14}OOH2\text{-}4$	10.0			Estimated
$C_6H_5OH + CH_3 = C_6H_5CH_3 + OH$	10.0			Estimated
$C_6H_5CH_3 + HO_2 = = C_6H_5CH_2j + H_2O_2$	3.16			Estimated
$C_6H_5CH_2j + HO_2 = C_6H_5CH_2Oj + OH$	7.94			Estimated
$C_4H_9OH + OH = C4H_8OH\text{-}1 + H_2O$	10.0			Estimated
$C_4H_9OH + OH = C4H_8OH\text{-}3 + H_2O$	10.0			Estimated
$C_4H_9OH + OH = C4H_8OH\text{-}4 + H_2O$	10.0			Estimated
$C_4H_9OH + HO_2 = C4H_8OH\text{-}1 + H_2O_2$	10.0			Estimated
$C_4H_8OH\text{-}1 + O_2 = C_3H_7CHO + HO_2$	10.0			Estimated
$C_4H_8OH\text{-}1 + O_2 = C4H_8OH\text{-}1O_2$	10.0			Estimated
$C_4H_8OH\text{-}1O_2 = C4H_7OH\text{-}1OOH\text{-}3$	10.0			Estimated
$C_4H_8OH\text{-}3O_2 = C4H_7OH\text{-}3OOH\text{-}1$	10.0			Estimated
$C_4H_8OH\text{-}1O_2 = C4H_7OH1\text{-}1 + HO_2$	10.0			Estimated
$C4H_7OH\text{-}3OOH\text{-}1 + O_2 = nC_4KET13 + HO_2$	10.0			Estimated
$C4H_7OH\text{-}3OOH\text{-}1 + O_2 = C4H_7OH\text{-}3OOH\text{-}1O_2$	10.0			Estimated